

Chapter 3

EGOE(1+2)-s: Pairing Correlations

3.1 Introduction

Pairing correlations play very important role in finite interacting Fermi systems such as nuclei [Ho-07,Ka-00], small metallic grains [Pa-02,Sc-08], quantum dots [Lu-01,Al-05] and so on. The EGOE(1+2)-s discussed in Chapter 2 provides a model for understanding general structures generated by pairing correlations [Pa-02,Al-05]. We adopt an algebraic approach to pairing rather than the BCS approach. Our purpose in this chapter is to study first the pairing symmetry in the space defined by EGOE(1+2)-s and then the measures for pairing, using EGOE(1+2)-s ensemble, that are of interest for nuclei (see [Ho-07]), quantum dots and small metallic grains (see [Sc-08]). In the space defined by EGOE(1+2)-s ensemble, pairing symmetry is defined by the algebra $U(2\Omega) \supset Sp(2\Omega) \supset SO(\Omega) \otimes SU_S(2)$. Starting with the details of this algebra we show that the state density generated by the pairing Hamiltonian will be a highly skewed distribution. In contrast, the partial densities over pairing subspaces follow Gaussian form and the propagation formulas for their centroids and variances, defined over subspaces given by the algebra $U(2\Omega) \supset Sp(2\Omega) \supset SO(\Omega) \otimes SU_S(2)$, are derived. Pair transfer strength sum as a function of excitation energy (for fixed S), a statistic for onset of chaos, is shown to follow, for low spins, the form derived for spinless fermion systems. The parameters defining this form are easy to calculate using propagation equations. In addition, we consider a quantity in terms of gs energies, giving conductance peak spacings in mesoscopic systems at low temperatures, and study its distribution over EGOE(1+2)-s by including both pairing and exchange interactions.

All the results presented in this chapter are published in [Ma-09, Ma-10].

3.2 $U(2\Omega) \supset Sp(2\Omega) \supset SO(\Omega) \otimes SU_S(2)$ Pairing Symmetry

Pairing algebra to be discussed here is presumably familiar to others. However to our knowledge the details presented here are not reported elsewhere (for a short related discussion see [Fl-64]). Note that, we drop the “hat” symbol over \hat{H} , \hat{h} and \hat{V} when there is no confusion as in Chapter 2.

Consider m fermions distributed in Ω number of sp levels each with spin $\mathbf{s} = 1/2$. Therefore total number of sp states is $N = 2\Omega$ and they are denoted by $a_{i,\mathbf{s}=\frac{1}{2},m_s}^\dagger |0\rangle = |i, \mathbf{s} = \frac{1}{2}, m_s = \pm \frac{1}{2}\rangle$ with $i = 1, 2, \dots, \Omega$. Similarly,

$$\frac{1}{\sqrt{1 + \delta_{i,j}}} \left(a_{i,\mathbf{s}=\frac{1}{2}}^\dagger a_{j,\mathbf{s}=\frac{1}{2}}^\dagger \right)_{m_s}^s |0\rangle = \left| \left(i, \mathbf{s} = \frac{1}{2}; j, \mathbf{s} = \frac{1}{2} \right) s, m_s \right\rangle$$

denotes two-particle antisymmetric states with the two-particle in the levels i and j and the two-particle spin $s = 0$ or 1 . From now on we will drop the index $\mathbf{s} = \frac{1}{2}$ for simplicity and then the two-particle antisymmetric states, in spin coupled representation, are

$$|(i, j) s, m_s\rangle = \frac{1}{\sqrt{1 + \delta_{i,j}}} \left(a_i^\dagger a_j^\dagger \right)_{m_s}^s |0\rangle.$$

In constructing EGOE(1+2)-s, only spin invariant Hamiltonians are considered. Thus the m -particle states carry good spin(S) quantum number [Ko-06, Tu-06]. Now the pair creation operator P_i for the level i and the generalized pair creation operator (over the Ω levels) P are

$$P = \frac{1}{\sqrt{2}} \sum_i \left(a_i^\dagger a_i^\dagger \right)^0 = \sum_i P_i, \quad P^\dagger = -\frac{1}{\sqrt{2}} \sum_i (\bar{a}_i \bar{a}_i)^0. \quad (3.2.1)$$

In Eq. (3.2.1), $\bar{a}_{i,\mathbf{s}=\frac{1}{2},m_s} = (-1)^{\frac{1}{2}+m_s} a_{i,\mathbf{s}=\frac{1}{2},-m_s}$. Therefore in the space defining EGOE(1+2)-s, the pairing Hamiltonian H_p and its two-particle matrix elements are,

$$H_p = P^2 = PP^\dagger, \quad (3.2.2)$$

$$\langle (k, \ell) s, m_s | H_p | (i, j) s', m_{s'} \rangle = \delta_{s,0} \delta_{i,j} \delta_{k,\ell} \delta_{s,s'} \delta_{m_s,m_{s'}}.$$

Note that the two-particle matrix elements of H_p (also true for H) are independent

of the m_s quantum number. With this, we will proceed to identify and analyze the pairing algebra. Firstly, it is easily seen that the $4\Omega^2$ number of one-body operators $u_\mu^r(i, j) = (a_i^\dagger \tilde{a}_j)^r_\mu$, $r = 0, 1$ generate $U(2\Omega)$ algebra; see Appendix D. They satisfy the following commutation relations,

$$\begin{aligned} \left[u_\mu^r(i, j), u_{\mu'}^{r'}(k, l) \right]_- &= \sum_{r''} (-1)^{r+r'} \langle r \mu r' \mu' | r'' \mu'' \rangle \sqrt{(2r+1)(2r'+1)} \\ &\times \left\{ \begin{array}{ccc} r & r' & r'' \\ 1/2 & 1/2 & 1/2 \end{array} \right\} \left[u_{\mu''}^{r''}(k, j) \delta_{il} - (-1)^{r+r'+r''} u_{\mu''}^{r''}(i, l) \delta_{jk} \right]. \end{aligned} \quad (3.2.3)$$

Here, $\langle \dots | \dots \rangle$ are CG coefficients and $\left\{ \dots \right\}$ are $6j$ -symbols. The $U(2\Omega)$ irreducible representations (irreps) are denoted trivially by the particle number m as they must be antisymmetric irreps $\{1^m\}$. The $2\Omega(\Omega - 1)$ number of operators $V_\mu^r(i, j)$,

$$V_\mu^r(i, j) = \sqrt{(-1)^{r+1}} \left[u_\mu^r(i, j) - (-1)^r u_\mu^r(j, i) \right]; \quad i > j, \quad r = 0, 1 \quad (3.2.4)$$

along with the 3Ω number of operators $u_\mu^1(i, i)$ form $Sp(2\Omega)$ subalgebra of $U(2\Omega)$ and this follows from the results in [Ko-06b]. Using anti-commutation relations for fermion creation and destruction operators and carrying out angular-momentum algebra [Ed-74], we have

$$\begin{aligned} &\left[(a_i^\dagger \tilde{a}_j)^k (a_j^\dagger \tilde{a}_i)^k \right]^0 \\ &= (-1)^k \sqrt{\frac{2k+1}{2j+1}} (a_i^\dagger \tilde{a}_i)^0 - \sum_{k'} \chi \left\{ \begin{array}{ccc} 1/2 & 1/2 & k \\ 1/2 & 1/2 & k \\ k' & k' & 0 \end{array} \right\} \left[(a_i^\dagger a_j^\dagger)^{k'} (\tilde{a}_j \tilde{a}_i)^{k'} \right]^0, \\ &\left[(a_i^\dagger \tilde{a}_j)^k (a_i^\dagger \tilde{a}_j)^k \right]^0 = -\chi \left\{ \begin{array}{ccc} 1/2 & 1/2 & k \\ 1/2 & 1/2 & k \\ 0 & 0 & 0 \end{array} \right\} (a_i^\dagger a_i^\dagger)^0 (\tilde{a}_j \tilde{a}_j)^0. \end{aligned} \quad (3.2.5)$$

Here, $\chi \{ \dots \}$ are $9j$ coefficients (they are not $9j$ -symbols). Note that

$$\chi \left\{ \begin{array}{ccc} 1/2 & 1/2 & k \\ 1/2 & 1/2 & k \\ s & s & 0 \end{array} \right\} = \sqrt{\frac{2s+1}{4}} \text{ for } k=0, \quad (3.2.6)$$

$$= \sqrt{\frac{2s+1}{3}} \left[\frac{3}{2} - s(s+1) \right] \text{ for } k=1.$$

We will show that the irreps of $Sp(2\Omega)$ algebra are uniquely labeled by the seniority quantum number 'v' discussed in the context of identical particle pairing in nuclear structure [Ta-93] and they in turn define the eigenvalues of H_p . The quadratic Casimir operators of the $U(2\Omega)$ and $Sp(2\Omega)$ algebras are [Ko-06b],

$$C_2[U(2\Omega)] = \sum_{i,j,r} u^r(i,j) \cdot u^r(j,i), \quad (3.2.7)$$

$$C_2[Sp(2\Omega)] = 2 \sum_i u^1(i,i) \cdot u^1(i,i) + \sum_{i>j,r} V^r(i,j) \cdot V^r(i,j).$$

Simplifying these expressions using relations in Eqs. (3.2.5) and (3.2.6) [with \hat{n} being the number operator], we have

$$C_2[U(2\Omega)] = 2\hat{n}\Omega - 2 \sum_i P_i P_i^\dagger - \sum_{i \neq j, s} \sqrt{2s+1} [s(s+1) - 1] \left[(a_i^\dagger a_j^\dagger)^s (\bar{a}_j \bar{a}_i)^s \right]^0,$$

$$C_2[Sp(2\Omega)] = (2\Omega + 1)\hat{n} - 6 \sum_i P_i P_i^\dagger - 4 \sum_{i>j} (P_i P_j^\dagger + P_j P_i^\dagger)$$

$$- \sum_{i \neq j, s} \sqrt{2s+1} [s(s+1) - 1] \left[(a_i^\dagger a_j^\dagger)^s (\bar{a}_j \bar{a}_i)^s \right]^0,$$

$$\Rightarrow C_2[U(2\Omega)] - C_2[Sp(2\Omega)] = 4 P P^\dagger - \hat{n}. \quad (3.2.8)$$

It is also seen that the operators P , P^\dagger and P_0 form $SU(2)$ algebra,

$$[P, P^\dagger] = \hat{n} - \Omega = 2 P_0, \quad [P_0, P] = P, \quad [P_0, P^\dagger] = -P^\dagger. \quad (3.2.9)$$

The corresponding spin is called quasi-spin Q . As M_Q , the P_0 eigenvalue, is $(m -$

$\Omega)/2$, we obtain $Q = (\Omega - \nu)/2$. Then, for $m \leq \Omega$, ν take values $\nu = m, m-2, \dots, 0$ or 1 . Therefore eigenvalues of the pairing Hamiltonian H_p are given by,

$$E_p(m, \nu, S) = \langle H_p \rangle^{m, \nu, S} = \langle PP^\dagger \rangle^{m, \nu, S} = \frac{1}{4}(m - \nu)(2\Omega + 2 - m - \nu). \quad (3.2.10)$$

As $\langle C_2[U(2\Omega)] \rangle^{1^m} = m(2\Omega + 1 - m)$, Eqs. (3.2.8) and (3.2.10) will give

$$C_2[Sp(2\Omega)] = 2\nu \left(\Omega + 1 - \frac{\nu}{2} \right). \quad (3.2.11)$$

Comparing Eq. (3.2.11) with the general formula for the eigenvalues of the quadratic Casimir invariant of $Sp(2\Omega)$ [Wy-74], it follows that the seniority quantum number ' ν ' corresponds to totally antisymmetric irrep $\langle 1^\nu \rangle$ of $Sp(2\Omega)$. Thus $Sp(2\Omega)$ corresponds to $SU(2)$ quasi-spin algebra generated by (P, P^\dagger, P_0) . More explicitly,

$$|m, \nu, S, \alpha\rangle = \sqrt{\frac{(\Omega - \nu - p)!}{(\Omega - \nu)! p!}} P^p |m = \nu, \nu, S, \alpha\rangle; \quad p = \frac{m - \nu}{2}. \quad (3.2.12)$$

Thus the spin S is generated by ' ν ' free particles and therefore $\nu \geq 2S$. Then, for a given (m, S) we have

$$\nu = m, m-2, \dots, 2S, \quad (m \leq \Omega). \quad (3.2.13)$$

Number of states or dimension $D(m, \nu, S)$, without the $(2S + 1)$ degeneracy factor, for a fixed- (m, ν, S) is,

$$D(m, \nu, S) = d_f(\Omega, m = \nu, S) - d_f(\Omega, m = \nu - 2, S). \quad (3.2.14)$$

Note that the fixed- (m, S) dimensions $d_f(\Omega, m, S)$ are given by Eq. (2.2.2). Table 3.1 gives the reductions $m \rightarrow S \rightarrow \nu$, $D(m, \nu, S)$ and also $E_p(m, \nu, S)$ for some examples. Let us point out $Sp(2\Omega) \supset SO(\Omega) \otimes SU(2)$ but $SO(\Omega)$ carries no extra information. In fact there is one-to-one correspondence between the $Sp(2\Omega)$ chain and the alternative group-subgroup chain $U(2\Omega) \supset U(\Omega) \otimes SU(2) \supset SO(\Omega) \otimes SU(2)$. This is verified by comparing the results in Table 3.1 with the irrep reductions for $U(\Omega) \supset SO(\Omega)$ that are given in Appendix D. It is useful to note that Eqs. (3.2.10), (3.2.13) and (3.2.14) will allow one to construct the state density generated by the pairing Hamiltonian

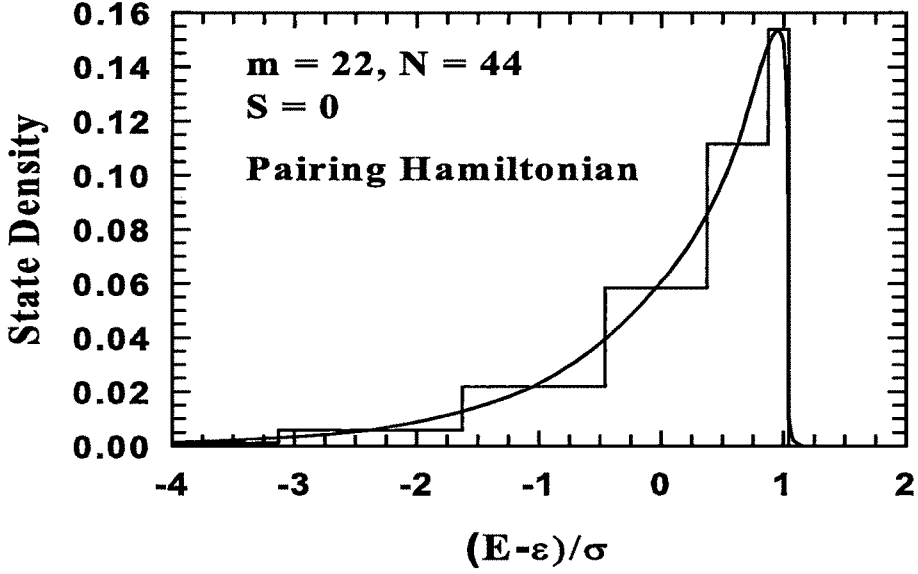


Figure 3.1: State density for the pairing Hamiltonian $H = -H_p$ for a system of 22 fermions in $\Omega = 22$ orbits ($N = 44$) and total spin $S = 0$. In the histogram, $\rho(E)$ for a given $\hat{E} = (E - \epsilon)/\sigma$ is plotted with \hat{E} as center with width given by $\Delta\hat{E} = \Delta E/\sigma$ (see Eq. (3.2.15) and the following discussion). The smooth curve is obtained by joining the center points to guide the eye. A similar plot was shown before by Ginocchio [Gi-80] but for a system of identical fermions in a large single- j shell.

$H = -H_p$. The dimensions $d_f(\Omega, m, S)$ and $D(m, v, S)$ along with the energy E_p of H_p will give the normalized density $\rho(E)$ to be

$$\rho_{(-H_p)}(E) = \frac{D(m, v, S)}{d_f(\Omega, m, S) \Delta E}; \quad \Delta E = E_p(m, v+1, S) - E_p(m, v-1, S) = \Omega - v + 1. \quad (3.2.15)$$

Figure 3.1 gives $\rho(\hat{E})$ vs \hat{E} plot for $\Omega = 22$ (i.e., $N = 44$), $m = 22$ and $S = 0$. For this system, the spectrum spread is 132 (note that $v_{max} = 22$), centroid $\epsilon \sim 5.7$ and width $\sigma \sim 6$; note that $\hat{E} = (E - \epsilon)/\sigma$. Clearly, it is a highly skewed distribution (see also the $\alpha = 0$ plot in Fig. 3.4 ahead).

3.3 Fixed- (m, v, S) Partial Densities and their Centroids and Variances

Expansion of a given $|m, v, S, \alpha\rangle$ basis state in terms of the H eigenstates $|E; (m, S)\rangle$, with the expansion coefficients being $C_E^{m, v, S, \alpha}$ will allow us to define the fixed- (m, v, S)

Table 3.1: Classification of states in the $U(2\Omega) \supset Sp(2\Omega) \supset SO(\Omega) \otimes SU_5(2)$ limit for $\Omega = 6$ with $m = 0 - 6$ and $\Omega = 8$ with $m = 6 - 8$. Given are (m, S, v) labels, the corresponding dimensions $D(m, v, S)$ and eigenvalues $E_p(m, v, S)$. Note that $\sum_{v,S}(2S+1)D(m, v, S) = \binom{2\Omega}{m}$ and $\sum_v D(m, v, S) = d_f(\Omega, m, S)$.

Ω	m	S	v	$D(m, v, S)$	$E_p(m, v, S)$	Ω	m	S	v	$D(m, v, S)$	$E_p(m, v, S)$					
6	0	0	0	1	0	8	6	0	6	840	0					
			1	6	0				4	300	4					
			2	20	0				2	35	12					
	3	$\frac{1}{2}$	0	0	1				6	0	1	18				
				1	15				0	1	6	1134	0			
				2	64				0	4	350	4				
				3	6				5	2	28	10				
				4	20				0	2	6	350	0			
				5	84				0	4	70	4				
	4	0	0	2	20				4	3	6	28	0			
				0	1				10	7	$\frac{1}{2}$	7	1344	0		
				1	90				0	5	840	3				
				2	15				4	3	160	8				
				4	15				0	1	8	15				
				5	$\frac{1}{2}$				5	5	140	0	$\frac{3}{2}$	7	840	0
										3	64	3	5	448	3	
										1	6	8	3	56	8	
										5	64	0	$\frac{5}{2}$	7	160	0
										3	20	3	5	56	3	
	5	6	0							$\frac{7}{2}$	7	8	0			
	6	0	6	6	70				0	8	0	8	8	588	0	
4				84	2	6	840	2								
2				20	6	4	300	6								
0				1	12	2	35	12								
1				84	0	0	1	20								
4				90	2	1	8	840	0							
2				15	6	6	1134	2								
6				20	0	4	350	6								
4				15	2	2	28	12								
3				6	1	0	0	2	8				300	0		
						6	350	2	6				350	2		
						4	70	6	4				70	6		
						8	35	0	3				8	35	0	
						6	28	2	6				28	2		
						8	1	0	4				8	1	0	

partial densities $\rho^{m,v,S}(E)$,

$$\rho^{m,v,S}(E) = \langle \delta(H - E) \rangle^{m,v,S} = \frac{1}{D(m,v,S)} \sum_{\alpha} |C_E^{m,v,S,\alpha}|^2 \quad (3.3.1)$$

$$\Rightarrow I^{m,v,S}(E) = D(m,v,S) \rho^{m,v,S}(E) = \sum_{\alpha} |C_E^{m,v,S,\alpha}|^2 .$$

Often it is convenient to use total densities $I(E)$ rather than the normalized densities $\rho(E)$. It is important to note that fixed- (m, S) density of states $\rho^{m,S}(E)$ decompose into a sum of fixed- (m, v, S) partial densities,

$$\rho^{m,S}(E) = \sum_v \frac{D(m,v,S)}{d_f(\Omega, m, S)} \rho^{m,v,S}(E) \quad (3.3.2)$$

$$\Rightarrow I^{m,S}(E) = \sum_v I^{m,v,S}(E) .$$

The partial densities are defined over broken symmetry subspaces and they are also called 'strength functions' or 'local density of states' [Ko-01, Ko-03]. Partial densities $\rho^{m,v,S}(E)$ give intensity distribution of a given basis state $|m, v, S\rangle$ over the eigenstates $|E\rangle$, i.e., distribution of the expansion coefficients $|C_E^{m,v,S}|^2$ vs E . The partial densities have same structure as that for the strength functions defined in Eq. (2.5.2) as partial sums over the strength functions give partial densities. We will also encounter partial densities in Chapter 5.

In the $\lambda > \lambda_F$ region, as discussed in Chapter 2, strength functions take Gaussian form and therefore partial densities are expected to be Gaussian in this region. Extension of this result to EGOE(1+2)- J [Pa-07] with subspaces defined by the pairing Hamiltonian, i.e., fixed- (m, v, J) partial densities are Gaussian is often used in nuclear physics [Qu-74, Qu-77]. In Fig. 3.2 we present tests of this assumption for EGOE(1+2)- s with J replaced by S . In order to discuss these results, we will start with the EGOE(1+2)- s Hamiltonian defined by Eq. (2.2.1). We choose, in all the calculations reported in this chapter, $\epsilon_i = i + (1/i)$, $i = 1, 2, \dots, \Omega$ and $\lambda_0 = \lambda_1 = \lambda = 0.3$. Results in Chapter 2 confirm that $\lambda = 0.3$ corresponds to strong coupling region. Before going further, let us add that we will later consider extensions of H with the inclusion of pairing and exchange interactions (they are not random). For a $\Omega = m = 8$ system

with 50 members, we have extracted the partial densities $\rho^{m,v,S}(E)$ in Eq. (3.3.1) by numerically constructing the H matrix in good S basis and then changing it into good (m, v, S) basis with an auxiliary diagonalization of H_p in the good S basis. Results for the ensemble averaged partial densities are shown for $S = 0$ and 1 in Fig. 3.2 and the results are compared with the Gaussian (\mathcal{G}) and ED corrected Gaussian forms given by Eq. (2.3.2). From the results in Fig. 3.2, it is seen that the agreement between the exact and ED corrected Gaussians is excellent. For $v = 0$ (this is one dimensional) the deviations are some what larger. Similar results are also obtained for a smaller example (these are not shown in the figure) with $\Omega = m = 6$ and $S = 0, 1$ and for this system we have carried out calculations with 500 members. This shows fixed- (m, v, S) partial densities take close to Gaussian form, just as fixed- (m, S) densities, in the strong coupling region. Thus the EGOE(1+2)-s densities follow EGOE(1+2) even in pairing subspaces. This is a result assumed in statistical nuclear spectroscopy (see for example [Da-80, Fr-82]).

For constructing Gaussian partial (m, v, S) densities, we need fixed- (m, v, S) centroids $E_c(m, v, S) = \langle H \rangle^{m,v,S}$ and variances $\sigma^2(m, v, S) = \langle H^2 \rangle^{m,v,S} - [E_c(m, v, S)]^2$. An important result here is, these parameters can be calculated for any (Ω, m, v, S) with $m > 4$ without recourse to H matrix construction in (m, S) spaces. This derives from the fact that simple (Casimir) propagation is possible for $E_c(m, v, S)$ in terms of the corresponding E_c for $m \leq 2$ and for $\sigma^2(m, v, S)$ in terms of the corresponding σ^2 for $m \leq 4$. From Table 3.1 one can see that the number of (m, v, S) irreps Λ_i is 5 for m up to 2 and there are 5 simple scalar operators \widehat{C}_i of maximum body rank 2, $\widehat{C}_i = 1, \hat{n}, \binom{\hat{n}}{2}, H_p,$ and \hat{S}^2 for $i = 1 - 5$, respectively. Note that $\langle H_p \rangle^{m,v,S}$ and $\langle \hat{S}^2 \rangle^{m,v,S}$ are $E_p(m, v, S)$ [see Eq. (3.2.10)] and $S(S+1)$, respectively. More remarkable is that, for $m \leq 4$, the number of (m, v, S) irreps Y_i is 14 as seen from Table 3.1 and also the available simple scalars $\widehat{\mathcal{E}}_i$ of maximum body rank 4 are exactly 14. These are $\widehat{\mathcal{E}}_i = 1, \hat{n}, \binom{\hat{n}}{2}, \binom{\hat{n}}{3}, \binom{\hat{n}}{4}, H_p, \hat{n}H_p, \binom{\hat{n}}{2}H_p, (H_p)^2, H_p\hat{S}^2, \hat{S}^2, \hat{n}\hat{S}^2, \binom{\hat{n}}{2}\hat{S}^2$ and $(\hat{S}^2)^2$ for $i = 1 - 14$, respectively. Therefore, the spectral variances over (m, v, S) spaces propagate simply and they will be linear combinations of the eigenvalues of the 14 operators above. The constants in the expansion will follow from the variances for $m \leq 4$. Then, fixed- (m, v, S) energy centroids with $\mathcal{S}^2 = S(S+1)$, $X(m, S) = m(m+2) - 4S(S+1)$ and

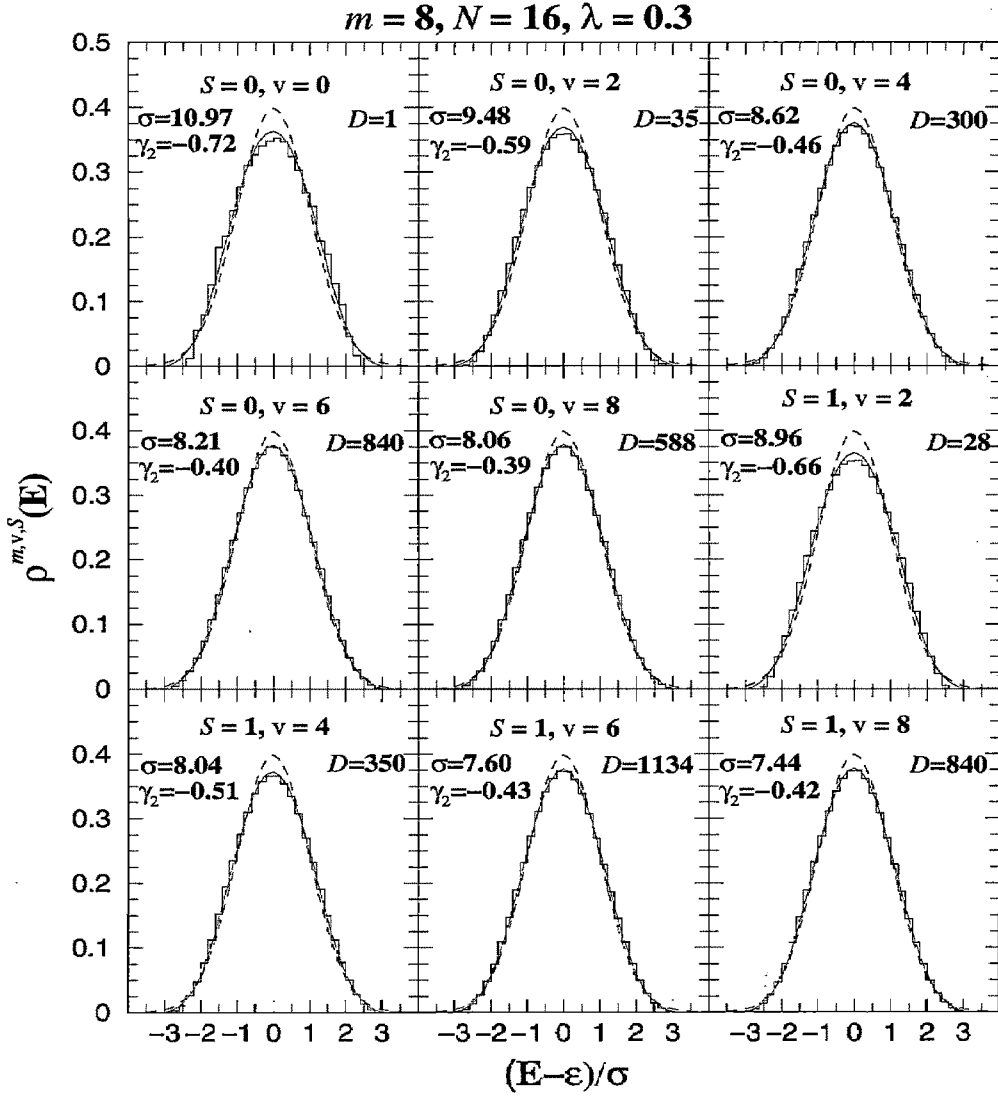


Figure 3.2: Partial densities $\rho^{m,v,S}(E)$ vs E for a EGOE(1+2)-s ensemble H defined in the text. The values of (v, S) , dimension D , width σ and γ_2 for the densities are given in the figure. Note that $\gamma_1 \sim 0$ in all cases. The energies E are zero centered with respect to the centroid ϵ and scaled with the width σ of $\rho^{m,v,S}(E)$. The histograms (with 0.2 bin size) are exact results, dashed curves are Gaussians and the continuous curves are Edgeworth corrected Gaussians. See text for further details.

$Y(m, S) = m(m-2) - 4S(S+1)$, are given by

$$\langle H \rangle^{m,v,S} = E_c(m, v, S) = a_0 + a_1 m + a_2 \binom{m}{2} + a_3 \mathcal{S}^2 + a_4 E_p(m, v, S) \quad (3.3.3)$$

$$\Rightarrow E_c(m, v, S) = \frac{1}{2}(m-1)(m-2) E_c(0, 0, 0) - m(m-2) E_c(1, 1, \frac{1}{2})$$

$$\begin{aligned}
& + \frac{1}{8\Omega} [-8E_p(m, \nu, S) + \Omega X(m, S)] E_c(2, 2, 0) + \frac{1}{\Omega} E_p(m, \nu, S) E_c(2, 0, 0) \\
& + \frac{1}{8} [4m(m-2) - Y(m, S)] E_c(2, 2, 1).
\end{aligned}$$

Similarly, fixed- (m, ν, S) spectral variances are

$$\begin{aligned}
\langle H^2 \rangle^{m, \nu, S} &= \frac{1}{24} (m-1)(m-2)(m-3)(m-4) \langle H^2 \rangle^{0,0,0} \\
& - \frac{1}{6} m(m-2)(m-3)(m-4) \langle H^2 \rangle^{1,1,\frac{1}{2}} \\
& + \frac{1}{16\Omega} (m-3)(m-4) [\Omega X(m, S) - 8E_p(m, \nu, S)] \langle H^2 \rangle^{2,2,0} \\
& + \frac{1}{2\Omega} (m-3)(m-4) E_p(m, \nu, S) \langle H^2 \rangle^{2,0,0} \\
& + \frac{1}{16} (m-3)(m-4) [3m(m-2) + 4\mathcal{S}^2] \langle H^2 \rangle^{2,2,1} \\
& - \frac{(m-2)(m-4)}{12(\Omega-1)} [(\Omega-1)X(m, S) - 12E_p(m, \nu, S)] \langle H^2 \rangle^{3,3,\frac{1}{2}} \\
& - \frac{1}{\Omega-1} (m-2)(m-4) E_p(m, \nu, S) \langle H^2 \rangle^{3,1,\frac{1}{2}} \tag{3.3.4} \\
& - \frac{1}{12} (m-2)(m-4) [m(m-4) + 4\mathcal{S}^2] \langle H^2 \rangle^{3,3,\frac{3}{2}} \\
& + \frac{1}{192(\Omega-2)(\Omega-1)} \left[96 \{E_p(m, \nu, S)\}^2 + 24 \{-(\Omega-1)m^2 + 2(\Omega+1)m \right. \\
& \left. + 4(\Omega-1)\mathcal{S}^2 - 4(\Omega+2)\} E_p(m, \nu, S) \right. \\
& \left. + (\Omega-1)(\Omega-2)X(m, S)Y(m, S) \right] \langle H^2 \rangle^{4,4,0} \\
& + \frac{1}{8\Omega(\Omega-2)} E_p(m, \nu, S) \\
& \times [\Omega\{m(m-2) - 4\mathcal{S}^2 + 8\} - 8\{E_p(m, \nu, S) + m-2\}] \langle H^2 \rangle^{4,2,0}
\end{aligned}$$

$$\begin{aligned}
& + \frac{1}{2\Omega(\Omega-1)} E_p(m, v, S) \{E_p(m, v, S) + m - \Omega - 2\} \langle H^2 \rangle^{4,0,0} \\
& + \frac{[3m(m-6) + 4\mathcal{S}^2 + 24]}{128(\Omega-2)} \\
& \times [(\Omega-2)X(m, S) - 16E_p(m, v, S)] \langle H^2 \rangle^{4,4,1} \\
& + \frac{1}{8(\Omega-2)} E_p(m, v, S) [3m(m-6) + 4\mathcal{S}^2 + 24] \langle H^2 \rangle^{4,2,1} \\
& + \frac{1}{384} [16(\mathcal{S}^2)^2 + 40m^2\mathcal{S}^2 - 240m\mathcal{S}^2 + 288\mathcal{S}^2 \\
& + 5m(m-2)(m-4)(m-6)] \langle H^2 \rangle^{4,4,2}.
\end{aligned}$$

Using EGOE(1+2)-s computer codes, it is easy to construct, even for large Ω values, the input averages $\langle H \rangle^{m,v,S}$, $m \leq 2$ for centroids and $\langle H^2 \rangle^{m,v,S}$, $m \leq 4$ for variances propagation. For a 100 member ensemble with $\Omega = 12$ and m changing from 8 to 12, we have calculated, for three lowest spins (i.e., for even m , with $S = 0, 1$ and 2 and odd m with $S = \frac{1}{2}, \frac{3}{2}$ and $\frac{5}{2}$), the ensemble averaged variances using Eq. (3.3.4). We use the EGOE(1+2)-s Hamiltonian defined by Eq. (2.2.1) with $\lambda = 0.3$. The ensemble averaged centroids do not change with 'v' as expected and therefore we will discuss the structure of variances. The results are shown in Fig. 3.3. It is observed that as the 'v' value increases from $2S$ to m , there is decrease in the variances. However the dimensions increase as 'v' increases. For example, for $S = 0$ and $m = 10$ the widths and dimensions are $(\sigma, D) = (20.93, 1), (18.6, 77), (17, 1638), (16, 14014), (15.44, 55055),$ and $(15.17, 99099)$ for $v = 0, 2, \dots, 10$. The decrease in variances with increasing 'v' is necessary for the gs to be dominated by $v = 0$, i.e., by pairing structure. As we shall discuss later, this indeed happens. Going beyond the averages, we have also calculated the variation over the ensemble for both centroids and variances as they will give information about fluctuations and ergodicity [Br-81, Be-01a, Ko-07]. We have calculated the ensemble variances for these, say $\mathcal{V}^2[E_c(m, v, S)]$ and $\mathcal{V}^2[\sigma^2(m, v, S)]$, respectively and then the corresponding scaled widths $\Delta_c(m, v, S) = \mathcal{V}[E_c(m, v, S)] / \{\overline{\sigma^2(m, v, S)}\}^{1/2}$ and $\Delta_s(m, v, S) = \mathcal{V}[\sigma^2(m, v, S)] / \overline{\sigma^2(m, v, S)}$. It is observed that Δ_c varies from 5 – 7% for $m = 8$, 7 – 9% for $m = 9$, 8 – 10% for $m = 10$, 9 – 13% for $m = 11$ and 10 – 14% for

$N = 24$

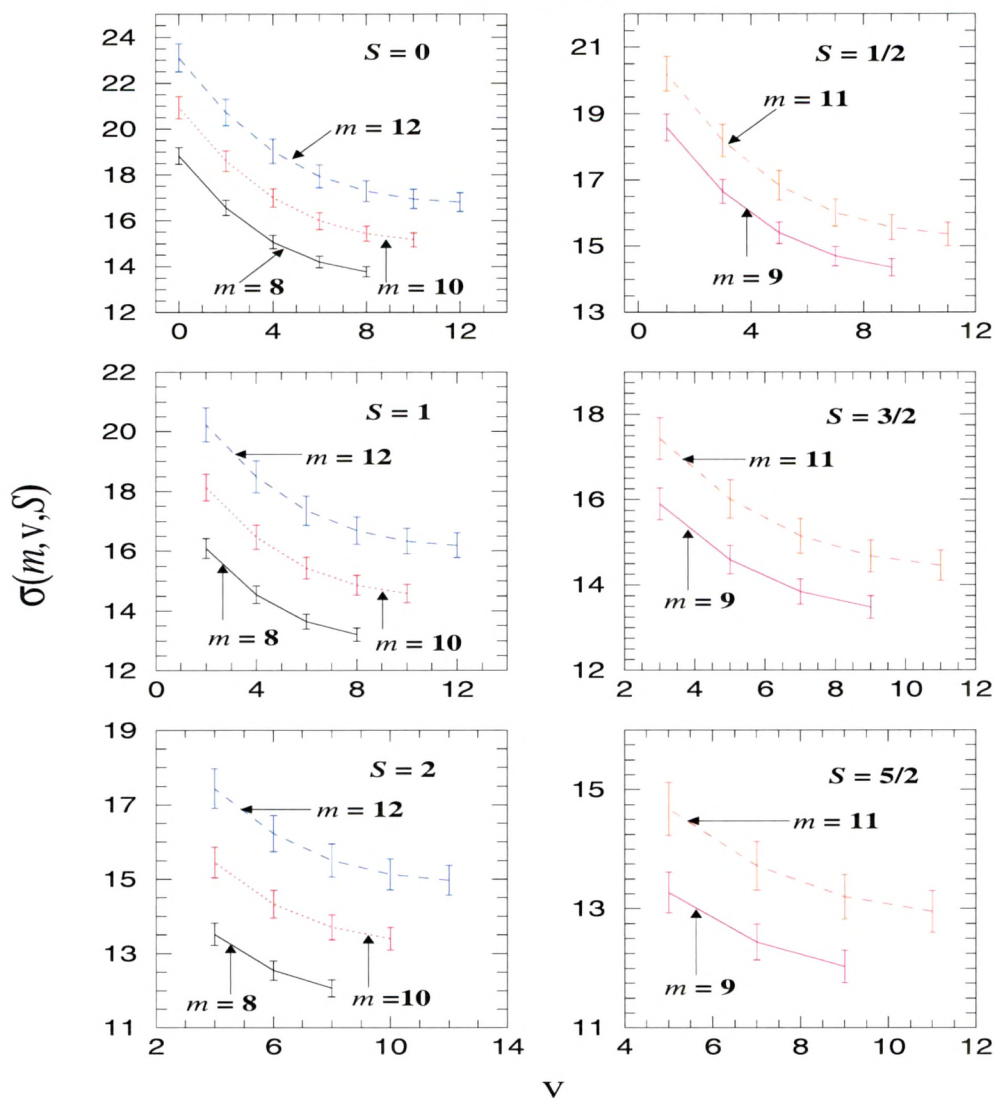


Figure 3.3: Ensemble averaged widths $\sigma(m, \nu, S)$ vs ' ν ' for EGOE(1+2)-s ensembles with $\Omega = 12$ and (m, S) values as given in the figures. Shown also in the figures are the r.m.s. deviations (over the ensemble) in the widths as error bars. For $m = 12$, the results are shifted by one unit to avoid overlapping of the error bars. See text for details.

$m = 12$. Thus centroid fluctuations are large just as the situation with EGOE for spinless fermion systems [Br-81, Be-01a]. However the variance fluctuations, as given by Δ_S are small, $\lesssim 5\%$. Therefore the widths are $\sigma(m, \nu, S) \sim \left[\overline{\sigma^2(m, \nu, S)} \right]^{1/2} \{1 \pm \frac{\Delta_S}{2}\}$. In Fig. 3.3 shown also are the fluctuations in widths.

3.4 Expectation Values $\langle PP^\dagger \rangle^E$ of the Pairing Operator as Signature of Chaos

A series of studies in the past, using Gamow-Teller, electric quadrupole and magnetic dipole transition operators, have established that transition strength sums can be considered as a statistic able to distinguish between regular and chaotic motion [Ko-99a, Go-01, Go-03]. Moreover, for EGOE(1+2) for spinless fermions in the strong coupling region, it is well understood that the strength sums vary with the excitation energy as ratio of two Gaussians [Fr-88, Ko-00, Ko-01, Ko-03]. This result was derived using the fact that (proved using the so-called binary correlation approximation) the transition strength densities, transition strengths multiplied by the state densities at the two energies involved, for EGOE(1+2) with $\lambda > \lambda_F$, take bivariate Gaussian form and hence, being the marginal densities, the strength sum densities (see ahead for the definition) will be Gaussian; see Chapter 7 for transition strength densities. It is now well established that the EGOE(1+2) (but not the GOE) provides a good description of strength sums in nuclear shell-model in the chaotic domain [Ko-99a, Go-01, Go-03]. Our interest is in calculating the expectation value of PP^\dagger over fixed- (m, S) spaces, which is a measure of the pairing correlations, and this is nothing but the strength sum for pair removal,

$$\langle PP^\dagger \rangle^{m,S,E} = \langle m, S, E | PP^\dagger | m, S, E \rangle = \sum_{E_f} \left| \langle m-2, S, E_f | P^\dagger | m, S, E \rangle \right|^2. \quad (3.4.1)$$

Recently Horoi and Zelevinsky [Ho-07] re-emphasized, in the context of pairing correlations in nuclei, the importance of $\langle PP^\dagger \rangle^E$ measure. Given a transition operator \mathcal{O} , in terms of the transition strength sum density $\rho_{\mathcal{O}^\dagger\mathcal{O}}(E)$, the expectation value $\langle \mathcal{O}^\dagger\mathcal{O} \rangle^E$ is

$$\langle \mathcal{O}^\dagger\mathcal{O} \rangle^E = \frac{\langle \mathcal{O}^\dagger\mathcal{O}\delta(H-E) \rangle}{\rho(E)} = \langle \mathcal{O}^\dagger\mathcal{O} \rangle \rho_{\mathcal{O}^\dagger\mathcal{O}}(E) / \rho(E). \quad (3.4.2)$$

As stated before, the normalized $\mathcal{O}^\dagger\mathcal{O}$ -density $\rho_{\mathcal{O}^\dagger\mathcal{O}}$ also takes Gaussian form for EGOE(1+2) with $\lambda > \lambda_F$ and it is defined by the centroid $\epsilon_{\mathcal{O}^\dagger\mathcal{O}} = \langle \mathcal{O}^\dagger\mathcal{O}H \rangle / \langle \mathcal{O}^\dagger\mathcal{O} \rangle$ and variance $\sigma_{\mathcal{O}^\dagger\mathcal{O}}^2 = \langle \mathcal{O}^\dagger\mathcal{O}H^2 \rangle / \langle \mathcal{O}^\dagger\mathcal{O} \rangle - \epsilon_{\mathcal{O}^\dagger\mathcal{O}}^2$. Similarly, skewness $\gamma_1(\mathcal{O}^\dagger\mathcal{O})$ and excess $\gamma_2(\mathcal{O}^\dagger\mathcal{O})$ for the $\mathcal{O}^\dagger\mathcal{O}$ -density are defined. The normalization factor $\langle \mathcal{O}^\dagger\mathcal{O} \rangle$ is the aver-

age value of $\mathcal{O}^\dagger \mathcal{O}$ over the complete space [in our examples this is fixed- (m, S) space]. Therefore the ensemble averaged strength sum density reduces to the ratio of two Gaussians or two ED corrected Gaussians [Fr-88, Ko-00, Ko-01, Ko-03],

$$\frac{\langle \mathcal{O}^\dagger \mathcal{O} \rangle^E}{\langle \mathcal{O}^\dagger \mathcal{O} \rangle} \xrightarrow{\text{EGOE}(1+2)} \rho_{\mathcal{O}^\dagger \mathcal{O}; \mathcal{G}}(E) / \rho_{\mathcal{G}}(E) \longrightarrow \rho_{\mathcal{O}^\dagger \mathcal{O}; \text{ED}}(E) / \rho_{\text{ED}}(E). \quad (3.4.3)$$

We will now test how well the EGOE(1+2) theory given by Eq. (3.4.3) extends to systems with spin, i.e., for EGOE(1+2)-s in the strong coupling regime and for the operator $\mathcal{O} = P^\dagger$. Note that in applying Eq. (3.4.3), all the averages and the densities will be over fixed- (m, S) spaces. As $H_p = PP^\dagger$ generates a highly skewed distribution for density of states, a priori it is expected that Eq. (3.4.3) may not be a good statistical formula for $\langle PP^\dagger \rangle^{m, S, E}$. Now we will investigate this using three numerical examples.

Just as in Section 3.3, first we have used the random EGOE(1+2)-s Hamiltonian defined in Eq. (2.2.1) and calculated $\langle PP^\dagger \rangle^{m, S, E}$ for various values of the λ parameter using a 500 member ensemble for 6 fermions ($m = 6$) in 6 orbits ($\Omega = 6$) and total spins $S = 0$ and 1. Results are shown in Fig. 3.4(a). Numerical results are compared with the EGOE(1+2) formula given by Eq. (3.4.3) both with and without ED corrections. For $\lambda = 0.1$, we have $\epsilon_{PP^\dagger} \sim 0$, $|\gamma_1(PP^\dagger)| \sim 0$, $\hat{\sigma}_{PP^\dagger} = \sigma_{PP^\dagger} / \sigma_H \sim 1.07$, $\gamma_2(PP^\dagger) \sim -0.47$ and $\langle PP^\dagger \rangle^{m, S} \sim 1.71$ for $S = 0$. Similarly, for $\lambda = 0.3$, $\gamma_2(PP^\dagger) \sim -0.55$ for $S = 0$ and ~ -0.63 for $S = 1$. Large values of $\gamma_2(PP^\dagger)$ imply that ED corrections are important in the examples considered and this is clearly seen in Fig. 3.4(a). The average value of PP^\dagger follows easily from the centroid formula given by Eq. (3.3.3),

$$\langle PP^\dagger \rangle^{m, S} = \frac{2}{\Omega + 1} \left\{ \frac{m(m+2)}{8} - \frac{S(S+1)}{2} \right\} \quad (3.4.4)$$

and this has been used to verify numerical calculations. As expected, the EGOE(1+2) smoothed form is not a good approximation to the exact results in the case of regular motion. Here there are large fluctuations due to approximate good quantum numbers and the level fluctuations will be close to that of Poisson. However, as λ increases and after the onset of chaos, in our example for $\lambda \gtrsim 0.1$, the interacting particle system is chaotic, giving a smoothed form for pair transfer strength sums (with fluctuations following GOE). This behavior is clearly seen in Fig. 3.4(a). To strengthen

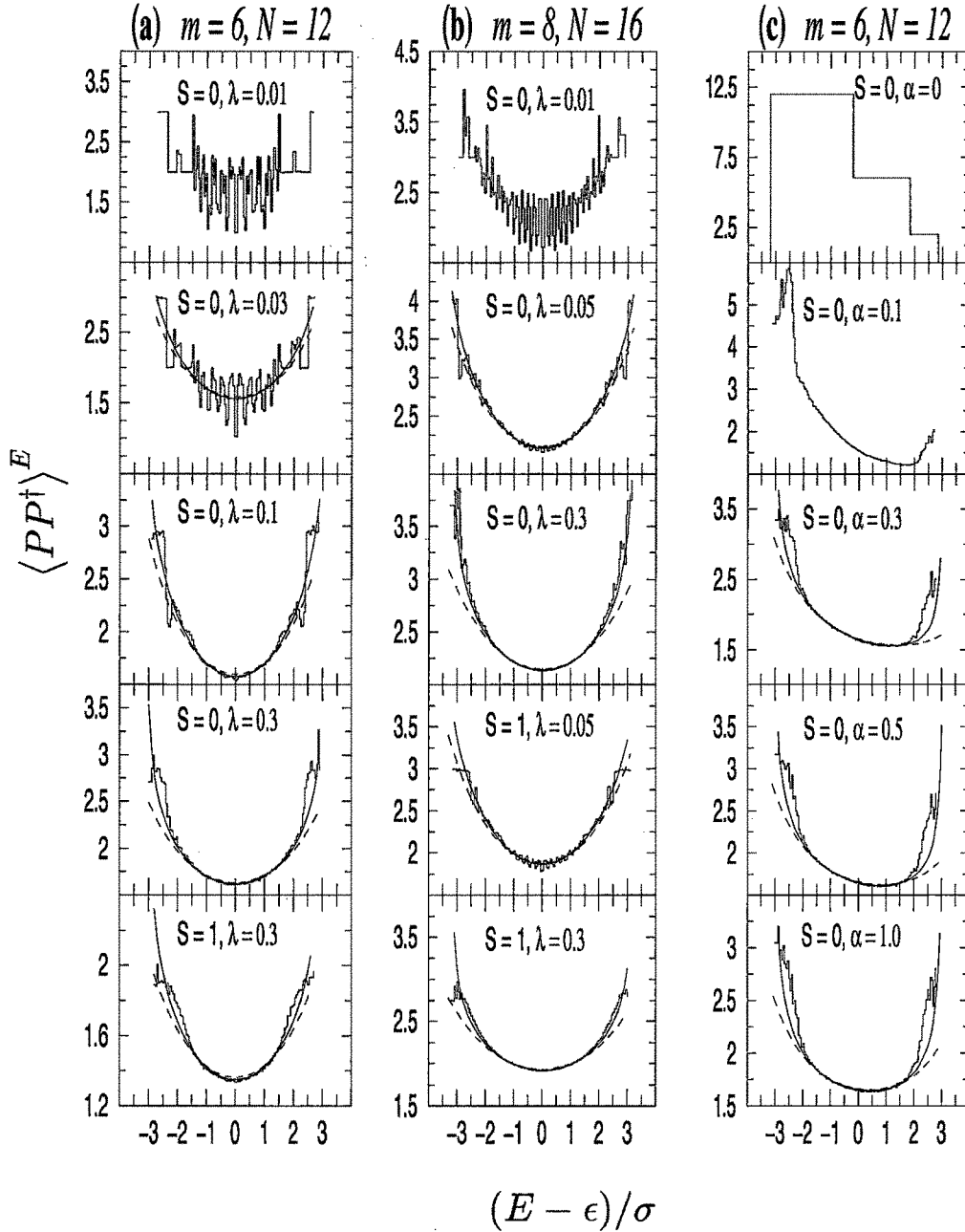


Figure 3.4: Ensemble averaged pairing expectation value $\langle PP^\dagger \rangle^{m,S,E}$ vs E for 3 different EGOE(1+2)-s examples. (a) For various values of λ in Eq. (2.2.1) with $\Omega = m = 6$ and $S = 0, 1$. (b) For various values of λ in Eq. (2.2.1) with $\Omega = m = 8$ and $S = 0, 1$. (c) For various values of α in Eq. (3.4.5) with $\Omega = m = 6$ and $S = 0$. Results are compared with the EGOE(1+2) formula given by Eq. (3.4.3), using Gaussian (dashed curves) and Edgeworth corrected Gaussian (solid curves) forms. The energies E are zero centered with respect to the centroid ϵ and scaled with the width σ of $\rho^{m,S}(E)$. See text for details.

these observations, calculations are repeated for a 50 member EGOE(1+2)-s ensemble with $\Omega = m = 8$ and total spins $S = 0$ and 1. The results are shown in Fig. 3.4(b). In this example, for $\lambda \gtrsim 0.05$ [note that for EGOE(1+2) there is scaling by $\sim 1/(m^2\Omega)$], the EGOE(1+2) form is in good agreement with numerical results. For $\lambda = 0.05$, we have $\epsilon_{PP^\dagger} \sim 0$, $|\gamma_1(PP^\dagger)| \sim 0$, $\hat{\sigma}_{PP^\dagger} \sim 1.06$, $\gamma_2(PP^\dagger) \sim -0.33$ and $\langle PP^\dagger \rangle^{m,S} \sim 2.22$ for $S = 0$. Similarly, $\gamma_2(PP^\dagger) \sim -0.37$ and $\langle PP^\dagger \rangle^{m,S} \sim 2$ for $S = 1$. For $\lambda = 0.3$, we have $\gamma_2(PP^\dagger) \sim -0.44$ for $S = 0$ and ~ -0.47 for $S = 1$. Thus, as seen from Figs. 3.4(a) and 3.4(b), pair expectation values follow, in the chaotic domain the simple EGOE(1+2) law given by Eq. (3.4.3). Also it is seen from the figures that at low energies the pair expectation value is large (but still much smaller than that for the pure pairing Hamiltonian) and then decreases as we go to the center (after that it will again increase as the space is finite). This trend is easily understood from the fact that $\hat{\sigma}_{PP^\dagger} > 1$. Also expectation values in the gs domain for $S = 0$ are always larger than for $S = 1$ and this is consistent with previously known results [Ho-07]. Thus random interactions, even in the chaotic domain, exhibit strong pairing correlations in the gs region and they decrease as we go up in the energy. Perhaps this explains the preponderance of 0^+ ground states seen in nuclear shell-model examples [Ze-04].

Going further, to understand the interplay between random interactions and pairing, calculations are carried out for $\langle PP^\dagger \rangle^{m,S,E}$ using the Hamiltonian,

$$H = \alpha [\{V^{s=0}\} + \{V^{s=1}\}] + [-H_p/\Omega] , \quad (3.4.5)$$

which explicitly contains the pairing part. Here we divide H_p by Ω so that the pairing gap (the gap between $v = 0$ and $v = 2$ states generated by H_p) is unity. Therefore the parameter α in Eq. (3.4.5) is the strength of the random part of the Hamiltonian in units of the pairing gap. Using a 500 member EGOE(1+2)-s ensemble, with H given by Eq. (3.4.5), for $\Omega = m = 6$ and $S = 0$, pair transfer strength sums are calculated as a function of energy for various α values. Results are shown in Fig. 3.4(c). For $\alpha = 0$, we have pure pairing Hamiltonian and this generates a staircase function. As the value of the strength of the random part increases to $\alpha > 0.3$, there is a transition to chaotic domain with $\langle PP^\dagger \rangle^{m,S,E}$ vs E taking a smoothed form (fluctuations being small and tending to that of GOE). The smooth behavior observed for $\alpha \geq 0.5$ is explained to

some extent by Eq. (3.4.3). For better description we use an expression (its derivation being straightforward) based on partial (m, v, S)-densities,

$$\langle PP^\dagger \rangle^{m,S,E} = \sum_{\mathbf{v}} \frac{I_{ED}^{m,\mathbf{v},S}(E)}{I_{ED}^{m,S}(E)} \langle PP^\dagger \rangle^{m,\mathbf{v},S}. \quad (3.4.6)$$

Note that the formula for $\langle PP^\dagger \rangle^{m,\mathbf{v},S}$ is given by Eq. (3.2.10) and $I_{ED}^{m,S}(E)$ is sum of $I_{ED}^{m,\mathbf{v},S}(E)$. Following Section 3.3, we have constructed the partial densities appearing in Eq. (3.4.6) as ED corrected Gaussians. The results obtained with these are shown in Fig. 3.4(c). It is seen that the agreements even at the spectrum ends are good (without partitioning the expectation values are found to be much larger than the exact results). It can be concluded from Fig. 3.4(c) that for α of the order 0.5 times the pairing gap, pairing effects get washed out and the structure of the expectation values is well explained by the EGOE(1+2) smoothed formula (3.4.6). It is plausible that unlike Eq. (3.4.3) that has worked well for the Hamiltonian defined by Eq. (2.2.1), the partitioned version given by Eq. (3.4.6) should be used for the Hamiltonian defined by Eq. (3.4.5) as this explicitly involves H_p , i.e., a regular part (as already discussed, H_p produces highly skewed density of states).

Partial densities give information about the composition, in terms of the 'v' quantum number, of the wavefunctions for a given E . Note that $f(\mathbf{v}) = I_{ED}^{m,\mathbf{v},S}(E) / I_{ED}^{m,S}(E)$ gives the fractional intensity of states with a given 'v' in the eigenstate with energy E ; see Eqs. (3.3.1) and (3.3.2). For the Hamiltonian in Eq. (3.4.5) with $\alpha = 0.3$, for $\hat{E} = -3$, the $f(\mathbf{v})$ for $\mathbf{v} = 0, 2, 4$ and 6 are 16%, 34%, 33%, and 17%, respectively. However for the random Hamiltonian given by Eq. (2.2.1) with $\lambda = 0.3$, the $f(\mathbf{v})$ values are 7%, 33%, 42%, and 18%. Thus in the gs domain, although the pair expectation values are enhanced (see Fig. 3.4), the wavefunctions have relatively small strength for $\mathbf{v} = 0$ states, i.e., they are not close to pure H_p eigenstates. This result is consistent with the nuclear shell-model results with random interactions, possessing J -symmetry, presented in [Zh-04]. Thus, some essential features of EGOE(1+2)- J are reproduced by EGOE(1+2)-s.

3.5 Distribution of $\Delta_2 = E_{gs}^{(m+1)} + E_{gs}^{(m-1)} - 2 E_{gs}^{(m)}$ With Pairing and Exchange Interactions

3.5.1 Brief introduction to mesoscopic systems

Mesoscopic systems are intermediate between microscopic systems (like nuclei and atoms) and macroscopic bulk matter. Quantum dots and ultrasmall metallic grains are good examples of mesoscopic systems whose transport properties can be measured [Im-97, Ja-01a]. When the electron's phase coherence length is comparable to or larger than the system size, the system is called mesoscopic. As the electron phase is preserved in mesoscopic systems, these are ideal to observe new phenomenon governed by the laws of quantum mechanics not observed in macroscopic conductors. Also, the transport properties of mesoscopic systems are readily measured with almost all system parameters (like the shape and size of the system, number of electrons in the system and the strength of coupling with the leads) under experimental control. The phase coherence length increases rapidly with decreasing temperature. For system size $\sim 100 \mu\text{m}$, the system becomes mesoscopic below $\sim 100 \text{ mK}$.

Quantum dots are artificial devices obtained by confining a finite number of electrons to regions with diameter $\sim 100 \text{ nm}$ by electrostatic potentials. Typically it consists of 10^9 real atoms but the number of mobile electrons is much lower, ~ 100 . Their level separation is $\sim 10^{-4} \text{ eV}$. If the transport in the quantum dot is dominated by electron scattering from impurities, the dot is said to be diffusive and if the transport is dominated by electron scattering from the structure boundaries, then dot is called ballistic. The coupling between a dot and its leads is experimentally controllable. When the dot is strongly coupled to the leads, the electron motion is classical and the dot is said to be open. In isolated or closed quantum dots, the coupling is weak and conductance occurs only by tunneling. Also the charge on the closed dot is quantized and they have discrete excitation spectrum. The tunneling of an electron into the dot is usually blocked by the classical Coulomb repulsion of the electrons already in the dot. This phenomenon is called Coulomb blockade. This repulsion can be overcome by changing the gate voltage. At appropriate gate voltage, the charge on the dot will fluctuate between m and $m+1$ electrons giving rise to a peak in the conductance. The

oscillations in conductance as a function of gate voltage are called Coulomb blockade oscillations. At sufficiently low temperatures, these oscillations turn into sharp peaks. In Coulomb blockade regime $kT \ll \Delta \ll E_c$, the tunneling occurs through a single resonance in the dot. Here, T is the temperature, Δ is the mean single particle level spacing and E_c is the charging energy. Ultrasmall metallic grains are small pieces of metals of size $\sim 2 - 10$ nm. The level separation for nm-size metallic grains is smaller than in quantum dots of similar size and thus experiments can easily probe the Coulomb blockade regime in quantum dots. Also, some of the phenomena observed in nm-size metallic grains are strikingly similar to those seen in quantum dots suggesting that quantum dots are generic systems for exploring physics of small coherent structures [Gu-98, Al-00a].

Although the quantum dots contain many electrons, their properties cannot be obtained by using thermodynamic limit. The description of transport through a quantum dot at low temperatures in terms of local material constants breaks down and the whole structure must be treated as a single coherent entity. The quantum limits of electrical conduction are revealed in quantum dots and conductivity exhibits statistical properties which reflect the presence of one-body chaos, quantum interference and electron-electron interaction. The transport properties of a quantum dot can be measured by coupling it to leads and passing current through the dot. The conductance through the dots displays mesoscopic fluctuations as a function of gate voltage, magnetic field and shape deformation. The techniques used to describe these fluctuations include semiclassical methods, random matrix theory and supersymmetric methods [Al-00a].

Mesoscopic fluctuations are universal dictated only by a few basic symmetries of the system. It is now widely appreciated that the universal conductance fluctuations are intimately related to the universal statistics of finite isolated quantum systems whose classical analogs are chaotic [Ko-01, Ko-03, Pa-07]. In describing transport through these coherent systems, we are interested in quantum manifestations of classical chaos. Scattering of electrons from impurities or irregular boundaries leads to single particle dynamics that are mostly chaotic. RMT describes the statistical fluctuations in the universal regime i.e., at energy scales below the Thouless energy $E = g\Delta$, g is the Thouless conductance. In this universal regime RMT addresses questions

about statistical behavior of eigenvalues and eigenfunctions rather than their individual description. We consider a closed mesoscopic system (quantum dot or small metallic grain) with chaotic single particle dynamics and with large Thouless conductance g . Such a structure is described by an effective Hamiltonian which comprises of a mean field and two-body interactions preserving spin degree of freedom. For chaotic isolated mesoscopic systems, randomness of single particle energies leads to randomness in effective interactions that are two-body in nature. Hence it is important to invoke the ideas of embedded ensembles to understand and also predict properties of these systems theoretically.

A realistic Hamiltonian for mesoscopic systems conserves total spin S and therefore includes a mean field one-body part, (random) two-body interaction, pairing H_p and exchange interaction \hat{S}^2 . In order to obtain physical interpretation of the \hat{S}^2 operator, we consider the space exchange or the Majorana operator M that exchanges the spatial coordinates of the particles and leaves the spin unchanged, i.e.,

$$M|i, \alpha; j, \beta\rangle = |j, \alpha; i, \beta\rangle. \quad (3.5.1)$$

In Eq. (3.5.1), labels i, j and α, β , respectively denote the spatial and spin labels. As the embedding algebra for EGOE(1+2)-s is $U(2\Omega) \supset U(\Omega) \otimes SU(2)$ and $|i, \alpha; j, \beta\rangle = (a_{i,\alpha}^\dagger a_{j,\beta}^\dagger)|0\rangle$, we have

$$2M = C_2[U(\Omega)] - \Omega \hat{n}. \quad (3.5.2)$$

In Eq. (3.5.2), $C_2[U(\Omega)] = \sum_{i,j,\alpha,\beta} a_{i,\alpha}^\dagger a_{j,\alpha} a_{j,\beta}^\dagger a_{i,\beta}$ is the quadratic Casimir invariant of the $U(\Omega)$ group,

$$C_2[U(\Omega)] = \hat{n}(\Omega + 2) - \frac{\hat{n}^2}{2} - \hat{S}^2. \quad (3.5.3)$$

Combining Eqs. (3.5.2) and (3.5.3), we have finally

$$M = -\hat{S}^2 - \hat{n} \left(\frac{\hat{n}}{4} - 1 \right). \quad (3.5.4)$$

Therefore, the interaction generated by the \hat{S}^2 operator is the exchange interaction with a number dependent term. This number dependent term becomes important when the particle number m changes. The H operator for isolated mesoscopic sys-

tems in universal regime has the form (with λ_p and λ_S being positive),

$$\{\widehat{H}(\lambda_0, \lambda_1, \lambda_p, \lambda_S)\} = \widehat{h}(1) + \lambda_0 \{\widehat{V}^{s=0}(2)\} + \lambda_1 \{\widehat{V}^{s=1}(2)\} - \lambda_p H_p - \lambda_S \widehat{S}^2. \quad (3.5.5)$$

The constant part arising due to charging energy E_c that depends on the number of fermions in the system can be easily incorporated in our model when required. For more details on two-body ensembles and mesoscopic systems see [Gu-98, Al-00a, Ko-01, Mi-00]. Before proceeding further, it is important to mention that, with the analytical formula for the propagator $P(\Omega, m, S)$ given by Eq. (2.3.12), EGOE(1+2)-s generates odd-even staggering in gs energies and also explains preponderance of gs with spin 0 (m even) for mesoscopic systems in a simple way. In other words, random interaction disfavor magnetized ground states; see Fig. 2.2. It is important to mention that even with the best available computing facilities, it is not yet feasible to numerically study the properties of large systems ($\Omega \gg 10$) modeled by EGOE(1+2)-s. As the minimum spin gs is favored by random interactions, the Stoner transition will be delayed in presence of a strong random two-body part in the Hamiltonian. The standard Stoner picture of ferromagnetism in itinerant systems is based on the competition between one-body kinetic energy [$h(1)$ in Eq. (3.5.5)] and the exchange interaction (\widehat{S}^2). The probability $P(S > 0)$ for the gs to be with $S > 0$ (for m even) is studied as a function of λ in Eq. (3.5.5) with $\lambda_p = 0$ and the results are given in Fig. 3.5. Thus EGOE(1+2)-s also explains the strong bias for low-spin ground states and the delayed gs magnetization by random two-body interactions.

3.5.2 Conductance peak spacing (Δ_2) distribution

Coulomb blockade oscillations yield detailed information about the energy and wavefunction statistics of mesoscopic systems. We consider a closed mesoscopic system and study the distribution $P(\Delta_2)$ of spacing Δ_2 between two neighboring conductance peaks at temperatures less than the average level spacing. Also our focus is in the strong interaction regime [$\lambda_0 = \lambda_1 = \lambda \geq 0.3$ in Eq. (3.5.5)] and we use fixed sp energies ϵ_i . The spacing Δ_2 between the peaks in conductance as a function of the gate voltage for $T \ll \Delta$ is second derivative of gs energies with respect to the number

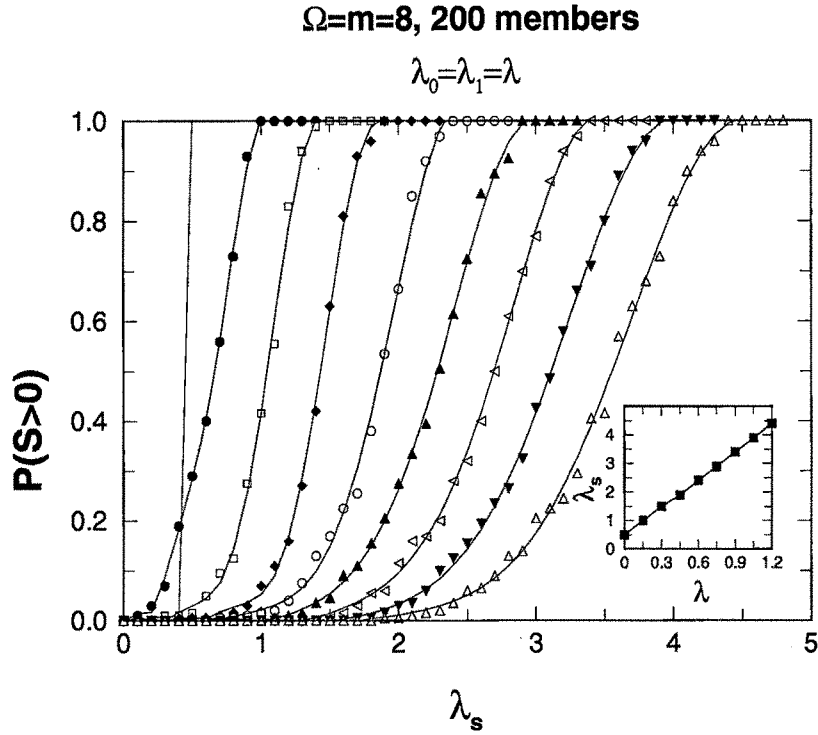


Figure 3.5: Probability $P(S > 0)$ for ground states to have $S > 0$ as a function of exchange interaction strength λ_s for $\lambda = 0$ to 1.2 in steps of 0.15; used here is $\hat{H}(\lambda, \lambda, 0, \lambda_s)$ defined by Eq. (3.5.5). The calculations are for 200 member EGOE(2)-s ensemble with $\Omega = m = 8$. Inset of figure shows the minimum exchange interaction strength λ_s required for the ground states to have $S > 0$ with 100% probability as a function of λ . It is seen from the results that the probability $P(S > 0)$ for gs to have $S > 0$ is very small when $\lambda > \lambda_s$ and it increases with increasing λ_s . The results clearly bring out the demagnetizing effect of random interaction. Similar calculations have been performed in the past for smaller systems with $\Omega = m = 6$ [Ko-06, Ja-01].

of particles,

$$\Delta_2 = E_{gs}^{(m+1)} + E_{gs}^{(m-1)} - 2 E_{gs}^{(m)}. \quad (3.5.6)$$

In Eq. (3.5.6), $E_{gs}^{(m)}$ is the gs energy for a m fermion system. The distribution $P(\Delta_2)$ has been used in the study of the distribution of conductance peak spacings in chaotic quantum dots [Al-05, Al-00, Al-01, Al-01a].

Let us first consider non-interacting spinless finite Fermi systems i.e., $H = h(1)$ and say the sp energies are ϵ_i ; $i = 1, 2, \dots, N$. Then Eq. (3.5.6) gives, by applying Pauli principle, $\Delta_2 = \epsilon_{m+1} - \epsilon_m$, irrespective of whether m is even or odd. For chaotic systems it is possible to consider sp energies drawn from GOE eigenvalues [Al-05, Al-00, Al-01, Al-01a]. Therefore $P(\Delta_2)$ corresponds to GOE spacing distribution $P_W(\Delta_2)$

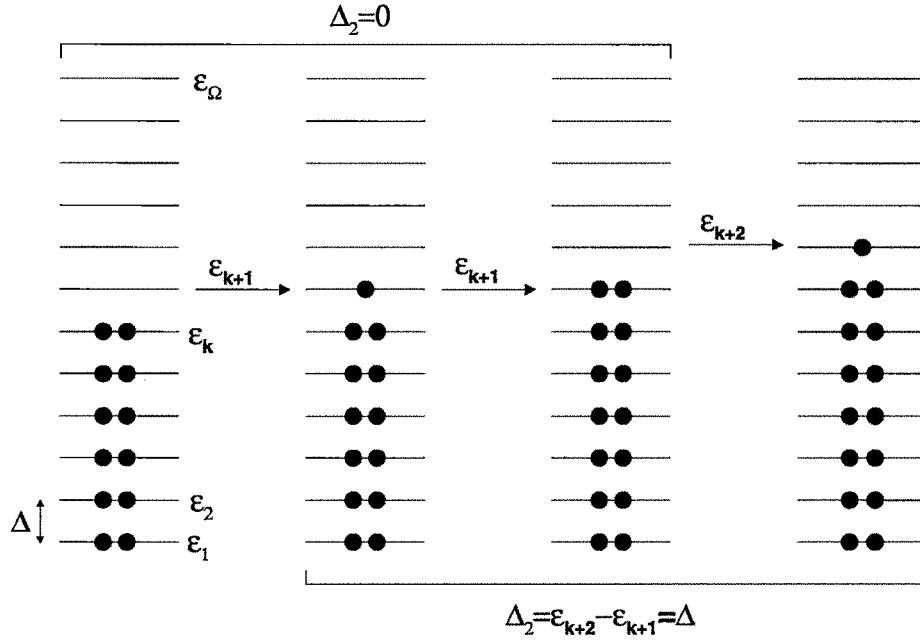


Figure 3.6: Figure showing Δ_2 values for systems with spin degree of freedom. For even-odd-odd transitions, $\Delta_2 = 0$ and for odd-even-odd transitions, $\Delta_2 = \Delta$. See text for details.

- the Wigner distribution. However recent experiments showed that $P(\Delta_2)$ is a Gaussian in many situations [Pa-98]. This calls for inclusion of two-body interactions and hence the importance of EGOE(1+2) (in [Al-00, Al-01, Al-01a] this is called RIMM) in the study of conductance fluctuations in mesoscopic systems. It was shown by Alhassid et al [Al-00, Al-01, Al-01a] that EGOE(1+2) indeed generates Gaussian form for $P(\Delta_2)$.

As discussed in Sec. 3.5.1, Hamiltonian for interacting electron systems conserves total spin S and thus it is important to consider sp levels that are doubly degenerate; i.e., spin degree of freedom should be included in H . Again, we start with non-interacting finite Fermi systems with sp energies ϵ_i , $i = 1, 2, \dots, \Omega$ and drawn from a GOE; total number of sp states $N = 2\Omega$. In this scenario Δ_2 depends on whether m is odd or even. For m odd, say $m = 2k + 1$, the $(m - 1)$ fermion gs energy $E_{gs}^{(m-1)} = 2\sum_{i=1}^k \epsilon_i$, $E_{gs}^{(m)} = E_{gs}^{(m-1)} + \epsilon_{k+1}$ and $E_{gs}^{(m+1)} = E_{gs}^{(m-1)} + 2\epsilon_{k+1}$ resulting in $\Delta_2 = 0$. Similar analysis for even $m = 2k$ yields $\Delta_2 = \epsilon_{k+1} - \epsilon_k$; note that $E_{gs}^{(m)} = 2\sum_{i=1}^k \epsilon_i$, $E_{gs}^{(m-1)} = E_{gs}^{(m)} - \epsilon_k$ and $E_{gs}^{(m+1)} = E_{gs}^{(m)} + \epsilon_{k+1}$. For odd m , Δ_2 corresponds to even-odd-odd transition and $P(\Delta_2)$ is a delta function. For even m , we have odd-even-odd transitions with $P(\Delta_2)$ following Wigner distribution. Figure 3.6 gives a pictorial illus-

tration for Δ_2 calculation for systems with spin. Therefore, by applying Pauli principle and using Eq. (3.5.6) gives $\Delta_2 = 0$ for m odd and $\Delta_2 = \epsilon_{k+1} - \epsilon_k$ for even m ($k = m/2$). As we need to include, for real systems, both even and odd m 's, inclusion of spin degree of freedom gives bimodal distribution for $P(\Delta_2)$,

$$P(\Delta_2) = \frac{1}{2} [\delta(\Delta_2) + P_W(\Delta_2)] . \quad (3.5.7)$$

Convolution of this bimodal form with a Gaussian has been used in the analysis of data for quantum dots obtained for situations that correspond to weak interactions [Lu-01]. This shows that spin degree of freedom and pairing correlations are important for mesoscopic systems. Hence, it is imperative to study $P(\Delta_2)$ with a Hamiltonian that includes mean field one-body part, (random) two-body interaction, exchange interaction and pairing (defined by H_p). Therefore we have carried out EGOE(1+2)-s calculations using the Hamiltonian given in Eq. (3.5.5) (with λ_p and λ_S being positive) and constructed $P(\Delta_2)$ by combining Δ_2 values obtained for both even and odd m values. Before discussing these model calculations let us mention that very recently, for small metallic grains, $P(\Delta_2)$ results are reported in [Sc-08]. These authors use a H consisting of pairing and exchange interactions just as in Eq. (3.5.5) but with sp energies of $h(1)$ drawn from GOE and a two-body interaction that is a function of m . More importantly a microscopic theory is used in [Sc-08] to construct $P(\Delta_2)$ at finite temperatures. When the pairing interaction is dominant (compared to exchange interaction), the distribution is found to be bimodal whereas the distribution becomes unimodal for strong exchange interaction. Following our discussion in the previous sections, here we present results for the distribution of Δ_2 defined by Eq. (3.5.6) with two values for m and using H defined by Eq. (3.5.5). We use fixed $h(1)$ as in the previous sections and $\lambda = 0.3$. Therefore our focus is in the strong interaction regime. Though our calculations are restrictive and the model is simpler, we will show that they reproduce all the essential features of $P(\Delta_2)$ reported in [Sc-08].

Using 1000 member EGOE(1+2)-s with H defined by Eq. (3.5.5), gs energies are calculated for $\lambda = 0.3$ and for various values of λ_p and λ_S by diagonalizing the Hamiltonian in good spin basis for $\Omega = 6$ and $m = 3, 4, 5$ and 6. Then Δ_2 is computed using Eq. (3.5.6) for $m = 4$ and 5 and combining these, normalized histograms for $P(\Delta_2)$

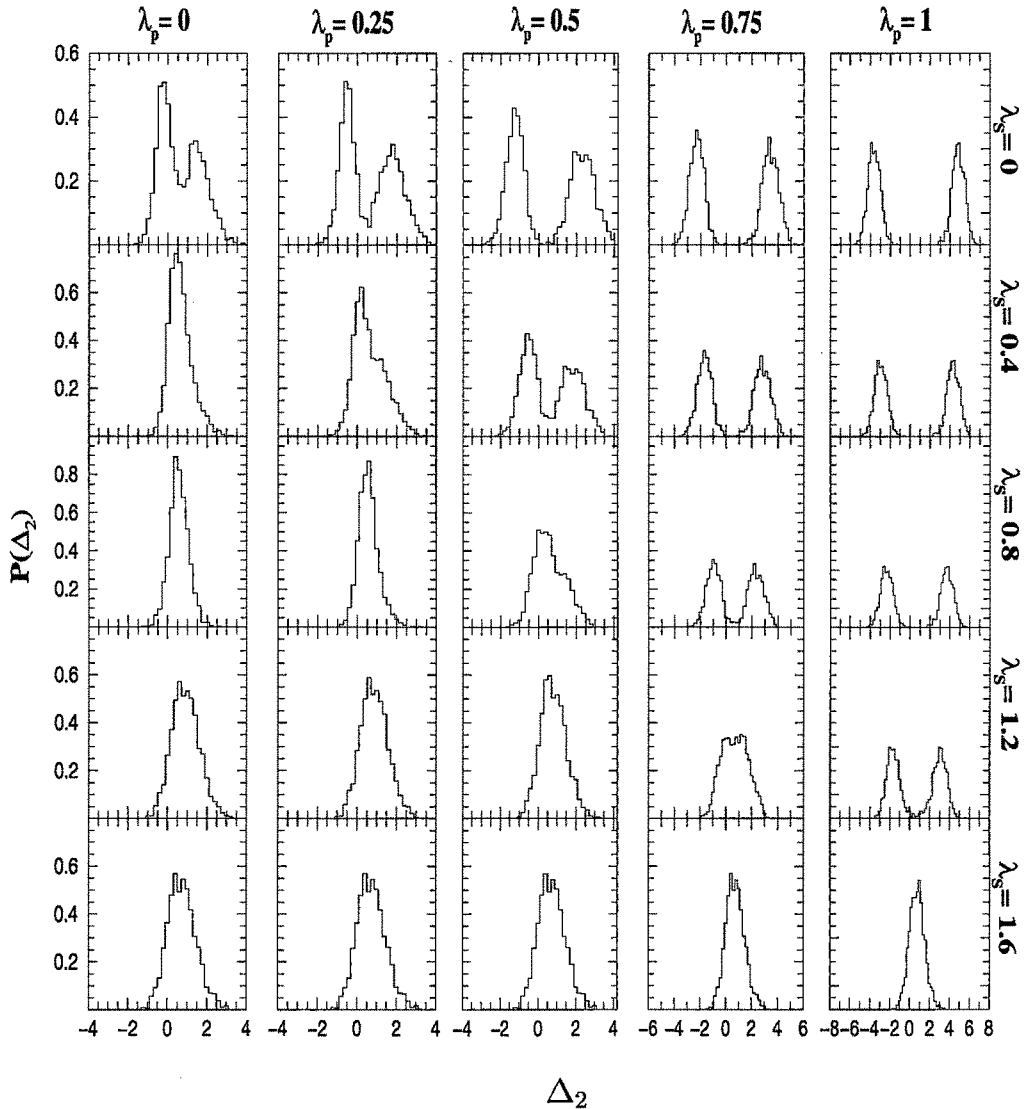


Figure 3.7: $P(\Delta_2)$ vs Δ_2 for various values of the pairing strength λ_p and exchange interaction strength λ_s for the EGOE(1+2)-s system defined in the text. The distributions $P(\Delta_2)$ are constructed (with bin size 0.2) by combining the results for Δ_2 with $m = 4$ and 5. See text for further details.

are constructed. Results in Fig. 3.7 show that strong pairing correlations ($\lambda_s = 0$) give rise to bimodal form for $P(\Delta_2)$ with the two modes well separated. Increasing the exchange interaction reduces the separation between the two parts and they overlap when exchange interaction is dominant and pairing is weak. In other words, pairing correlations help distinguish between m even and m odd in Eq. (3.5.6). These conclusions are close to the results in Fig. 1 of [Sc-08]. A qualitative understanding of these results follows from the centroids $\langle \Delta_2 \rangle$ of $P(\Delta_2)$ for each m generated by H_p

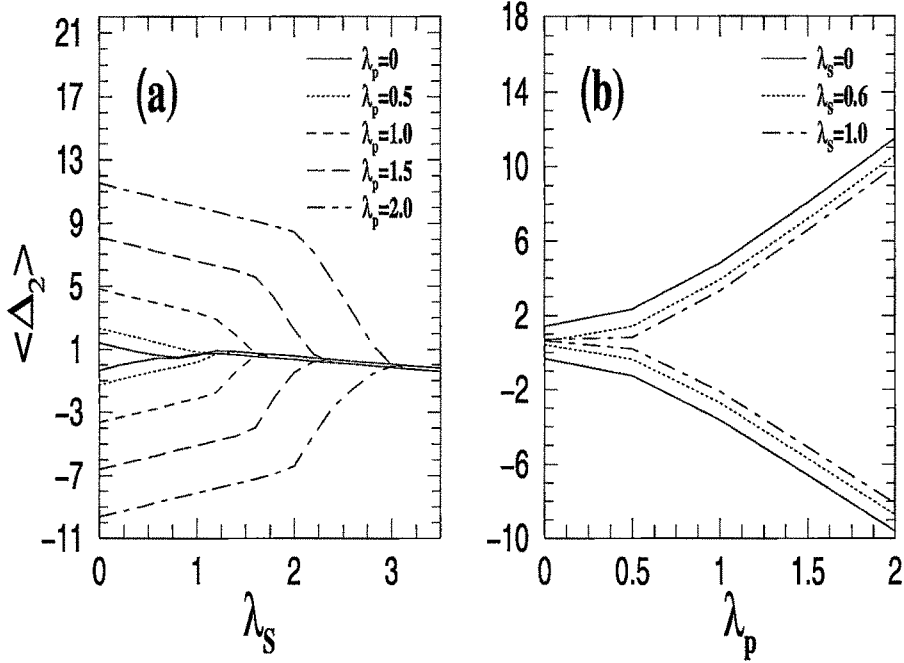


Figure 3.8: Average peak spacing $\langle \Delta_2 \rangle$ (a) as a function of exchange interaction strength λ_S for several values of pairing strength λ_p and (b) as a function of λ_p for several values of λ_S , for a 1000 member ensemble with $\Omega = 6$. The curves in the upper part correspond to $m = 4$ ($3 \rightarrow 4 \rightarrow 5$) and those in the lower part to $m = 5$ ($4 \rightarrow 5 \rightarrow 6$) in Eq. (3.5.6). See text for details.

and \hat{S}^2 terms in H . When pairing is relatively stronger ($\lambda_p \gg \lambda_S$), gs has minimum spin and thus $v = 0(1)$ for m even(odd) and when pairing is weaker ($\lambda_S \gg \lambda_p$), gs has maximum spin ($S = m/2$) and thus $v = m$. Using the pairing eigenvalues $E_p(m, v, S)$ given by Eq. (3.2.10), it is easily seen that for weak pairing, $\langle \Delta_2 \rangle = -\lambda_S/2$ for both m even and odd and for strong pairing, $\langle \Delta_2 \rangle = (\Omega + 1)\lambda_p - 3/2\lambda_S$ and $-\Omega\lambda_p + 3/2\lambda_S$ for even m and odd m , respectively. Therefore, for fixed λ_S , spacing between the peaks for $m = 4$ and $m = 5$ increases with sufficiently large λ_p values as seen in Fig. 3.7.

Figure 3.8(a) shows the variation of average peak spacing with exchange interaction strength λ_S for several λ_p values. The curves in the upper part correspond to $m = 4$ and those in the lower part to $m = 5$. As the exchange strength increases, the average peak spacing $\langle \Delta_2 \rangle$ is almost same for odd-even-odd and even-odd-even transitions. Value of average peak spacing and its variation with λ_S is different for odd-even-odd and even-odd-even transitions when pairing correlations are strong. The curve for fixed value of λ_p can be divided into two linear regions whose slopes can be determined considering only exchange interactions i.e., $E_{g_s} = C_0 - \lambda_S S(S+1)$. For weak exchange interaction strength, gs spin is $0(1/2)$ for m even(odd) and thus

for this linear region, $\langle \Delta_2 \rangle / \lambda_S \propto -3/2(3/2)$. The linear region where exchange interactions are dominant, $\langle \Delta_2 \rangle / \lambda_S \propto -1/2$ as gs spin is $m/2$. Figure 3.8(b) shows the variation of average peak spacing with pairing strength for several λ_S values. It clearly shows that the separation between the distributions becomes larger with increasing λ_p . These results are in good agreement with the numerically obtained results for the $P(\Delta_2)$ variation as a function of λ_p and λ_S in Fig. 3.7. Thus, EGOE(1+2)-s with H defined in Eq. (3.5.5) explains the interplay between exchange (favoring ferromagnetism) and pairing (favoring superconductivity) interaction in the Gaussian domain as expected in mesoscopic systems and can be used for investigating transport properties of mesoscopic systems.

3.6 Summary

Going beyond the results reported in Chapter 2 for the random matrix ensemble EGOE(1+2)-s, in the present chapter, further results are presented with focus on pairing correlations. Firstly, in the space defined by EGOE(1+2)-s ensemble, pairing symmetry defined by the algebra $U(2\Omega) \supset Sp(2\Omega) \supset SO(\Omega) \otimes SU_S(2)$ is identified and some of its properties are discussed. Using numerical calculations it is shown that in the strong coupling limit, partial densities defined over pairing subspaces are close to Gaussian form and propagation formulas for their centroids and variances are derived. As a part of understanding pairing correlations in finite Fermi systems, we have shown that pair transfer strength sums (used in nuclear structure) as a function of excitation energy (for fixed S), a statistic for onset of chaos (used in nuclei [Ho-07]), follows, for low spins, the form derived for spinless fermion systems i.e., it is close to a ratio of Gaussians. This is demonstrated using three detailed examples. Going further, we have considered a quantity in terms of gs energies, giving conductance peak spacings in mesoscopic systems at low temperatures, and studied its distribution over EGOE(1+2)-s by including both pairing and exchange interactions. We have shown that the random matrix model reproduces the main results that are observed recently in a realistic calculation for small metallic grains. Finally, results reported in this chapter establish that EGOE(1+2)-s can be used as a random matrix model for studying pairing correlations in finite quantum systems.